ELSEVIER

Thermochimica Acta 336 (1999) 27–40

thermochimica acta

www.elsevier.com/locate/tca

Temperature modulated differential scanning calorimetry. Part III. Effect of heat transfer on phase angle in quasi-isothermal ADSC

Zhong Jiang[a], Corrie T. Imrie[a], John M. Hutchinson[b,*]

[a]*Department of Chemistry, University of Aberdeen, Aberdeen AB24 3UE, UK*
[b]*Department of Engineering, King's College, University of Aberdeen, Aberdeen AB24 3UE, UK*

Received 27 November 1998; accepted 20 May 1999

Abstract

The effect of heat transfer on the phase measurements of alternating differential scanning calorimetry (ADSC, Mettler-Toledo) has been investigated, continuing previous work, using quasi-isothermal experiments. A new model for the prediction of the effects of heat transfer has been suggested in this work, and more closely simulates the practical conditions than did the earlier model. In particular, the reference sensor temperature is compared with the sample sensor temperature rather than with the sample temperature itself, as was used in the previous model. Both theoretical simulation and experimental results show that a phase angle is introduced simply by virtue of heat transfer effects, and that it depends on many experimental parameters. In particular, it is independent of the amplitude of temperature modulation, but depends strongly (and non-linearly) on the frequency and approximately linearly on the sample mass. To a large extent, these dependencies are well predicted by the theoretical model, which also predicts a strong influence of the heat transfer coefficient characterising the quality of the interface been sample and pan. It is shown that the use of a heat transfer fluid can largely eliminate the inconsistencies in the interfacial contact between sample and pan.

Keywords: Temperature modulated differential scanning calorimetry; Heat transfer; Phase angle; Polycarbonate; Quasi-isothermal

1. Introduction

Temperature modulated differential scanning calorimetry (TMDSC) is a new thermal analytical technique originally developed by Reading and co-workers [1–3], which is based on the idea of superimposing a periodically modulated temperature on the linear temperature programme used in conventional DSC. TMDSC can offer more information than conventional DSC and has considerable potential in the characterisation of inorganic, organic and polymeric materials. To date, much attention has been paid to its application to the study of the glass transition, with experimental work revealing a number of characteristic features in the TMDSC response e.g. [4–8] and with theoretical models predicting this response and aiding in its interpretation [9–11]. Other applications have included cold crystallisation [12], polymer blends [13,14], and the curing of thermosetting systems [15,16] and evaluation of activation energies [17], illustrating the advantages of TMDSC in separating closely occurring or overlapping transitions and in following directly the change in heat capacity during the cross-linking reaction.

*Corresponding author. Tel.: +44-1224-272791; fax: +44-1224-272497
E-mail address: j.m.hutchinson@eng.abdn.ac.uk (J.M. Hutchinson)

0040-6031/99/$ – see front matter
PII: S0040-6031(99)00138-0

Despite these successes of the technique, however, it is probably true to say that the full potential of TMDSC has yet to be realised. The reason for this is that some of the fundamental aspects are not yet entirely clear in general; these include, for example, the relationship between the phase angle and material properties, the physical significance of the specific heat capacities, and the effects of experimental conditions on the results.

In this last respect, it has been appreciated by some other researchers [18–20] that the heat transfer in the cell of TMDSC greatly affects the signals. In our earlier work of this series [21] we also examined the influence of heat transfer, in particular on the phase angle, and illustrated a procedure, following the idea of Schick and co-workers [19], for correcting the phase angle in the glass transition region by separating the instrumental effects from those caused by the transition itself. The basis for this procedure was a simple model suggested by Wunderlich et al. [18], which considered the phase angle between instrument and sample. Whilst this is a reasonable first approximation, and has the undoubted advantage of simplicity, it does not truly reflect the situation that prevails in TMDSC, most notably because it is not possible to measure the temperature of the sample itself.

In order to further our understanding of the problem of heat transfer in TMDSC, and hence to approach a more quantitative analysis of the technique, we present in this work the phase angle measurements predicted theoretically using a more refined model of the heat transfer situation, and measured experimentally using alternating DSC (ADSC, Mettler-Toledo, one of a number of commercial TMDSC instruments). The effects of heat transfer and experimental conditions on the ADSC response have been examined in particular in quasi-isothermal conditions in the glassy state for an amorphous polymer, polycarbonate.

2. Theory of TMDSC in quasi-isothermal conditions

2.1. Model A

From a simple analysis of heat flow, schematically illustrated in Fig. 1, Model A, Wunderlich et al. [18] derived a relationship between the phase angle and the mass and specific heat capacity of the sample, and the frequency of the temperature modulations. The heat flow from the DSC (temperature T_d) to the sample (temperature T_s) can be written as

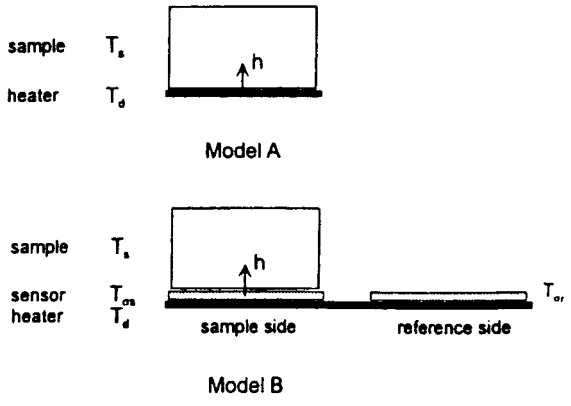

Fig. 1. Heat transfer models. Model A – suggested by Wunderlich; Model B – sensor temperatures included.

$$q = hA(T_d - T_s), \tag{1}$$

where h is a heat transfer coefficient. If no heat is lost from sample, then

$$q = mC_p\dot{T}_s, \tag{2}$$

where m and C_p are the mass and specific heat capacity of the sample, respectively, and $\dot{T}_s$ represents the time derivative of T_s. If a sinusoidal temperature modulation of T_d superimposed on a linear increase in temperature is expressed as

$$T_d = T_0 + \beta t + A_T \sin \omega t, \tag{3}$$

where T_0 is the initial temperature of the instrument (and sample) at time $t = 0$, β is the underlying heating rate, A_T is the temperature amplitude and ω is the angular frequency of temperature modulation, then the following differential equation for the temperature of the sample can be derived:

$$mC_p \frac{dT_s}{dt} = hA(T_0 + \beta t + A_T \sin \omega t - T_s). \tag{4}$$

This may be solved to give the steady state temperature modulation of the sample:

$$T_s = T_0 + \beta(t - \tau) + \frac{A_T}{\sqrt{1 + \omega^2\tau^2}} \sin(\omega t + \phi), \tag{5}$$

where τ is the time constant given by

$$\tau = \frac{mC_p}{hA}, \tag{6}$$

and ϕ is the phase angle given by

$$\phi = \arctan(-\omega\tau) = \arctan\left(-\frac{mC_p\omega}{hA}\right) \approx -\frac{mC_p\omega}{hA}. \tag{7}$$

Here, ϕ is the phase angle between the DSC and sample temperatures (the former leading the latter), but it also represents the phase angle between heating rate, from the derivative of Eq. (3), and the heat flow, from Eq. (2) (the former again leading the latter). From Eq. (7) it can be seen that, for small phase angles, ϕ is linearly related to m, C_p, and ω, and is inversely proportional to h.

The linear relationship between ϕ and C_p was used in our earlier work on polycarbonate [21], providing the basis for the correction of the phase angle in the glass transition region. Nevertheless, it should be recognised that this is only a first approximation to the real situation. Although the effect of heat transfer across the interface between DSC and sample has been included (by means of the heat transfer coefficient h), some key issues have not been considered. In particular, the real sample temperature can not be measured by any commercial TMDSC instrument. What is measured in practice are the temperatures of the sensors which are located beneath the sample and reference pans. In other words, the phase angle given by Eq. (7) is not exactly the experimentally measured phase angle although, as will be seen below, their features are to some extent quite similar.

2.2. Model B

A more realistic representation of the TMDSC would be to compare the temperatures of the sensors on the reference and sample sides of the cell. In this new model (see Fig. 1 – Model B), the reference side sensor temperature, $T_{\sigma r}$ is taken as the programmed temperature, identical to that of the DSC in Model A above:

$$T_{\sigma r} = T_0 + \beta t + A_T \sin\omega t. \tag{3a}$$

This temperature programme is achieved by virtue of a heater whose temperature may be written as

$$T_d = a_0 + b_0 t + c_0 e^{-t/\tau_0} + d_0 \sin\omega t + e_0 \cos\omega t. \tag{8}$$

Likewise, the sample side sensor temperature ($T_{\sigma s}$) and sample temperature (T_s) can be written, respectively, as:

$$T_{\sigma s} = a_1 + b_1 t + c_1 e^{-t/\tau_1} + d_1 \sin\omega t + e_1 \cos\omega t, \tag{9}$$

$$T_s = a_2 + b_2 t + c_2 e^{-t/\tau_2} + d_2 \sin\omega t + e_2 \cos\omega t, \tag{10}$$

and their heating rates as:

$$\dot{T}_{\sigma s} = b_1 - \frac{c_1}{\tau_1} e^{-t/\tau_1} + d_1\omega\cos\omega t - e_1\omega\sin\omega t, \tag{11}$$

$$\dot{T}_s = b_2 - \frac{c_2}{\tau_2} e^{-t/\tau_2} + d_2\omega\cos\omega t - e_2\omega\sin\omega t. \tag{12}$$

In Eqs. (8)–(12), the subscripted a, b, c, d and e are constants to be determined (see Appendix), with subscripts 0, 1, 2 representing heater, sample sensor and sample, respectively.

In order to clarify the derivation developed below, we define here the notation used. The heat transfer coefficient from sample side sensor to sample is denoted by h. The mass of the reference side sensor, sample side sensor and sample are denoted by $m_{\sigma r}$, $m_{\sigma s}$ and m_s, respectively. The same systematic subscripts are used for the specific heat capacity, C_p, and the thickness, L. The cross-sectional area of the sample is A.

We are concerned here with steady state conditions, and will therefore ignore the terms containing c_0, c_1, and c_2 in Eqs. (8)–(12). It is assumed that the heat flows in only one dimension, that is from heater to sensor to sample, or from heater to sensor on the reference side, and also that no heat is lost either from sensor to environment on the reference side, or from sample to environment on the sample side. Furthermore, heat flow from heater to sensors is considered to occur by conduction with no interface, whereas that from sensor to sample is controlled by the heat transfer coefficient h. Then, on the reference side, the heat flow from heater to sensor can be written

as follows:

$$q_{d\to\sigma r} = k_{\sigma r}\cdot A(T_d - T_{\sigma r}) / L_{\sigma r} = m_{\sigma r}C_{p,\sigma r}\dot{T}_{\sigma r}. \tag{13}$$

Since $T_{\sigma r}$ is the programmed temperature, given by Eq. (3)(a), the steady state heater temperature T_d may be written:

$$T_d = T_0 + \frac{m_{\sigma r}\cdot C_{p,\sigma r}\cdot L_{\sigma r}\cdot \beta}{k_{\sigma r}\cdot A} + \beta t + A_T \sin\omega t + \frac{m_{\sigma r}\cdot C_{p,\sigma r}\cdot L_{\sigma r}\cdot \omega\cdot A_T}{k_{\sigma r}\cdot A}\cos\omega t, \tag{14}$$

from which a_0, b_0, d_0, and e_0 may be identified by comparison with Eq. (8).

On the sample side, the heat flows from heater to sensor and from sensor to sample can be expressed, respectively, as:

$$q_{d\to\sigma s} = k_{\sigma s}\cdot A(T_d - T_{\sigma s}) / L_{\sigma s} \tag{15}$$

and

$$q_{\sigma s\to s} = h\cdot A(T_{\sigma s} - T_s) = m_s C_{p,s}\dot{T}_s. \tag{16}$$

The time derivative of the sensor temperature on the sample side may therefore be found from:

$$q_{d\to\sigma s} - q_{\sigma s\to s} = m_{\sigma s}\cdot C_{p,\sigma s}\cdot \dot{T}_{\sigma s}. \tag{17}$$

By substituting the general expressions for $T_{\sigma s}$ and T_s from Eqs. (9) and (10), respectively, into Eqs. (15)–(17), and equating coefficients, the subscripted constants *a*–*e* may be determined (see Appendix). From the resulting expressions for the temperature of the heater (T_d), sample side sensor ($T_{\sigma s}$) and sample (T_s) one can define a number of phase angles. In particular, the phase angle of the temperature of the sample sensor relative to the reference sensor can be expressed by (see Eq. (A.28)).

$$\phi_{\sigma s} = \arctan\left[\frac{-\omega P(1-\omega^2 QR)}{1+\omega^2(PQ+PR+Q^2+R^2)+\omega^4 Q^2R^2}\right],$$

where the quantities *P*, *Q* and *R* have been defined in Appendix A (see Eqs. (A.13)–(A.15).

From the above equation it can be seen that the phase angle depends in a more complex way on the experimental parameters than is predicted by the simpler Model A (Eq. (7)). At low frequency, when $\omega^2 \to 0$, $\phi_{\sigma s}$ can be seen to depend approximately linearly on the mass and specific heat capacity of the sample, and linearly also on the frequency, in the same way as the dependence predicted by Eq. (7). However, at higher frequencies these linear dependencies for $\phi_{\sigma s}$ are modified by the extra terms. Interestingly, the effect of increasing the heat transfer coefficient *h*, which enters in the denominator of the quantity *R*, can be seen to increase the absolute magnitude of $\phi_{\sigma s}$; in other words, the better is the heat transfer between sensor and sample, the greater is the magnitude of the phase angle $\phi_{\sigma s}$.

In Model B, the problem of heat transfer between DSC and sample is addressed while the temperature of the sample is assumed uniform through its thickness. A further refinement would be to allow for a temperature gradient to be introduced into the sample in Model B, by allowing for thermal conduction within the sample itself. From the same analytical procedure as was used in Model B one could derive an expression for the phase angle of the sample sensor temperature relative to that of the reference sensor temperature. However, when the sample is quite thin, as is the case in practical experiments, the results would not be much different from those from Model B, especially at the limit of low frequencies. Nevertheless, this analysis is in progress, and will be reported in a further paper.

In the present work, the theoretical simulations based on Eq. (A.28) have been carried out on MATLAB version 4.2, Copyright © 1984–1994 by The Mathworks. Quasi-isothermal experimental conditions have been used in the simulation. The frequency range investigated is up to 0.5 rad/s in order to examine the effects of heat transfer at high frequency. The following values were used for the various parameters: $k_\sigma = 0.6$ W/m K, $L_\sigma = 1$ mm, $A = 19.6$ mm^2, $m_\sigma = 30$ mg, $C_{p,\sigma} = 0.5$ J/g K, $m = 12.0$ mg and $C_{p,s} = 1.2$ J/g K.

3. Experimental

3.1. Materials

The polycarbonate samples were machined from extruded solid rod (Tecanat, Ensinger). The sample discs, with diameter 5 mm to suit the aluminium crucibles (pans) of the DSC, were turned and then parted on a lathe into discs of thickness 0.25, 0.50,

0.75, 1.00, 1.25 and 1.50 mm with corresponding masses about 6.0, 12.0, 18.0, 24.0, 30.0 and 36.0 mg. The density is approximately 1200 kg/m^3.

3.2. Quasi-isothermal ADSC modulated temperature programs

Quasi-isothermal ADSC experiments were performed at a constant temperature of 100°C, i.e. in the glassy state for polycarbonate, with a modulated temperature amplitude of 0.5 K; the period was varied between 12 and 1200 s. The intracooler was used for all measurements and nitrogen was always used as purge gas.

3.3. ADSC evaluation

Three separate ADSC runs were performed for every ADSC evaluation as follows: (1) empty run – without crucibles in either sample or reference positions; (2) blank run – a crucible with a lid in the sample position, and a crucible without lid in the reference position; (3) sample run – polycarbonate sample in the same crucible with the same lid (as for 2) in the sample position, and the same crucible, without lid (as for 2) in the reference position. The empty run is used for compensation of the cell asymmetry, while the blank run is used as an on-line calibration making use of the known specific heat capacity of aluminium and the small difference in mass of aluminium between sample and reference sides. It should be noted that the phase angle evaluated by the Mettler-Toledo analysis will usually be negative, except in the case of an exothermic reaction, indicating that the heat flow modulations lag behind the heating rate modulations.

4. Results and discussion

4.1. Theoretical simulations

Fig. 2 shows the relationship between phase angle ($\phi_{\sigma s}$) and modulation frequency (ω) for different

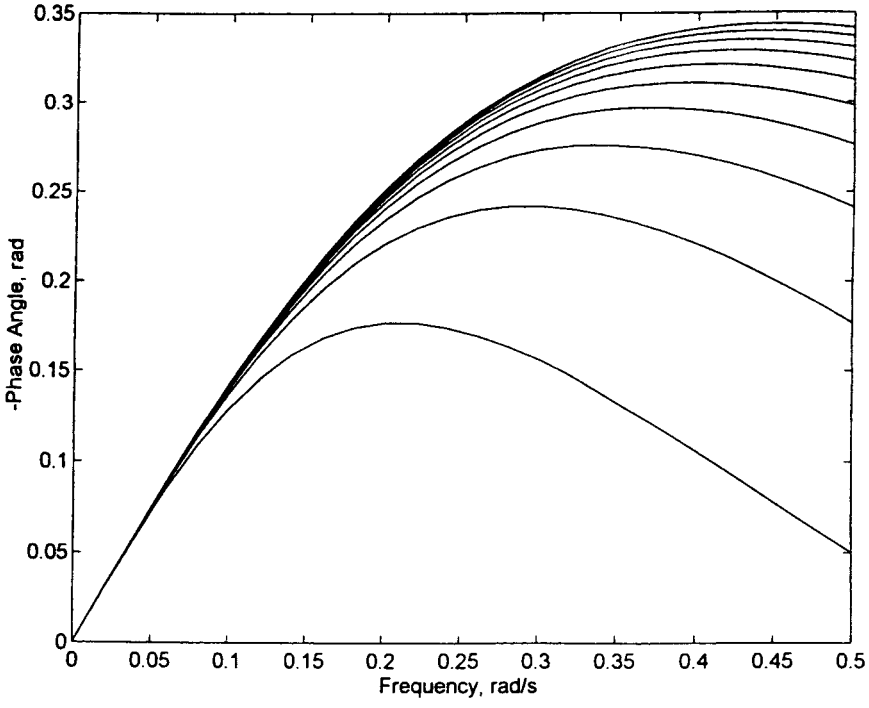

Fig. 2. Simulation of the effects of heat transfer coefficient h on the phase angle; h increases from 400 W/m^2 K (bottom) to 4000 W/m^2 K (top) with an interval of 400 W/m^2 K.

values of the heat transfer coefficient h. It can be seen that the phase angle not only depends on the modulation frequency, and in a complex way, but also is significantly influenced by the heat transfer conditions. With increasing frequency, $-\phi_{\sigma s}$ increases initially, then reaches a maximum value before decreasing; indeed, if the frequency is sufficiently high, $-\phi_{\sigma s}$ can eventually become negative, in other words the phase angle can become positive. The heat transfer coefficient between sensor and sample, h, influences both the value and frequency dependence of $-\phi_{\sigma s}$. On the one hand, the greater is the heat transfer coefficient, the larger is $-\phi_{\sigma s}$ at the same frequency; on the other hand, the maximum value of $-\phi_{\sigma s}$ appears at higher frequency as h increases.

These effects can be understood from Eq. (A.28) for the dependence of $-\phi_{\sigma s}$ on the frequency ω and on the experimental conditions. In particular, at low frequency this equation approximates to a linear relationship between $-\phi_{\sigma s}$ and ω, with slope P (see Eq. (A.13)) defined by the sample mass and specific heat capacity and by the thickness and thermal conductivity of the sensor. For given sensor properties, this slope is proportional to the mass and specific heat capacity of the sample.

For higher frequencies, $-\phi_{\sigma s}$ is reduced below this linear relationship as a result of both the $(1-\omega^2 QR)$ term in the numerator, which decreases as R increases, and also the denominator in Eq. (A.28), which increases as R increases from zero. This reduction is therefore greater the larger is the value of R (see Eq. (A.15)), and hence the smaller is the heat transfer coefficient. Interestingly, this means that the better is the thermal contact between sample and sensor the greater will be the measured value of the negative phase angle. At sufficiently high frequencies, the phase angle passes through a maximum and will eventually become positive, at a frequency given by $\omega^2 = 1/(QR)$. This ''cross-over'' frequency will therefore increase with decreasing R, in other words, with increasing heat transfer coefficient.

It is interesting to interpret the physical meaning of these observations. From the model, where it is assumed that there is no heat loss to the surroundings from either sample or reference side, we know that $T_{\sigma r}$ is affected only by the heat flow $q_{d\leftrightarrow\sigma s}$, whereas $T_{\sigma s}$ is influenced by both the heat flows $q_{d\leftrightarrow\sigma s}$ and $q_{\sigma s\leftrightarrow s}$. The double–headed arrows indicate that the heat flow may be in either direction, depending on the relative magnitudes of the relevant temperatures. Since $\phi_{\sigma s}$ is the phase difference between $T_{\sigma s}$ and $T_{\sigma r}$, increasing the modulation frequency (ω) would always increase $-\phi_{\sigma s}$ if the heat flow were only from T_d to $T_{\sigma s}$ to T_s. However, the heat flow in the reverse direction from T_s to $T_{\sigma s}$ to T_d can change the trend under some circumstances. Fig. 3 shows the temperature modulations, during just one cycle, for T_d, $T_{\sigma r}$, $T_{\sigma s}$ and T_s at frequencies of (a) 0.1, (b) 0.2, (c) 0.4, and (d) 0.8 rad/s. It can be seen that, at the lowest frequencies (below 0.1 and 0.2 rad/s, Fig. 3(a) and (b)), both $\phi_{\sigma s}$ and ϕ_s increase, and at the same time the temperature amplitudes decrease, and more so for T_s than for $T_{\sigma s}$. These phase lags and changes in amplitude lead to the development of some special intervals as regards the temperature modulations. In Fig. 3(b), for example, in the interval between 1.97 and 2.17 rad, $T_{\sigma s}$ is higher than both T_d and T_s, while in the interval between 5.11 and 5.31 rad, $T_{\sigma s}$ is lower than both T_d and T_s. In these intervals, the sample sensor is either cooled or heated, respectively, by both heater and sample during the relevant cooling or heating part of the cycle. As the frequency is increased, both intervals develop, such that for $\omega = 0.4$ rad (Fig. 3(c)), they lie between 2.02 and 2.41 rad, and between 5.16 and 5.55 rad; for $\omega = 0.8$ (Fig. 3(d)), they lie between 1.87 and 2.55 rad, and between 5.01 and 5.69 rad. Consequently, the simultaneous cooling and heating by both heater and sample shift the phase of $T_{\sigma s}$ forward. When the shifted phase offsets the increase of the phase lag between $T_{\sigma s}$ and $T_{\sigma r}$ (at around 0.2 rad/s, see Fig. 2), the maximum in $-\phi_{\sigma s}$ is obtained. When the shifted phase eventually offsets the phase lag between $T_{\sigma s}$ and $T_{\sigma r}$ (at around 0.6 rad/s in this case), the cross-over to positive values of $\phi_{\sigma s}$ is achieved.

Besides the dependence of the phase angle on the quality of the interface between sensor and sample, already discussed with reference to Fig. 2, the behaviour of the phase angle is also influenced significantly by the properties of the sensor and of the sample (refer to Eqs. (A.13)–(A.15)). With respect to the former, Fig. 4 predicts the influence of the thermal conductivity of the sensor on the phase angle. It can be seen that increasing the thermal conductivity reduces the phase angle in general, at least for frequencies less than that at which the maximum in the phase angle occurs, and also leads to a decrease in the maximum

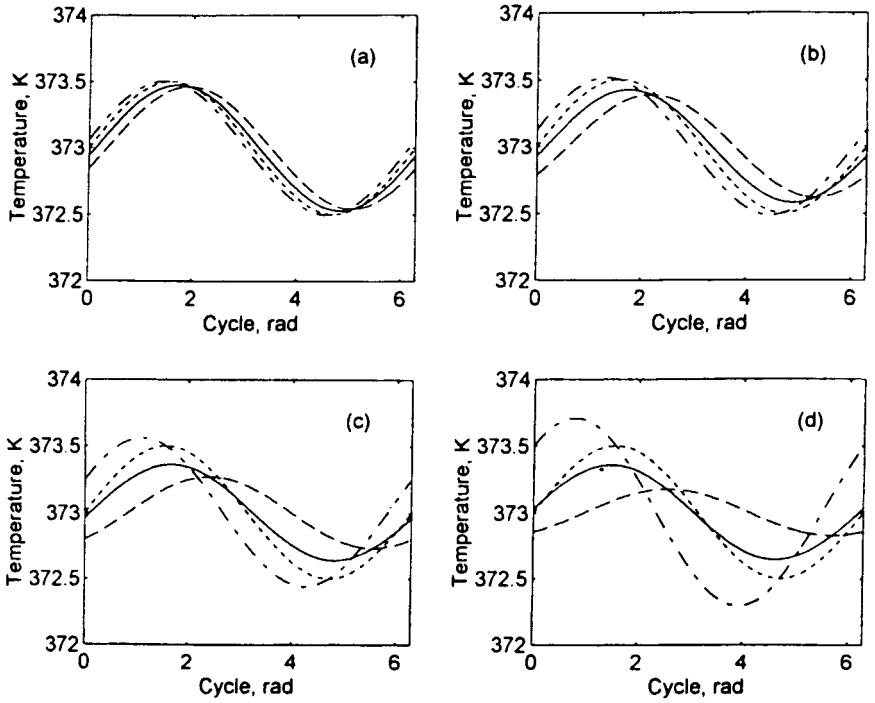

Fig. 3. Simulations of $T_{\sigma r}$ (–), T_d (-·), $T_{\sigma s}$ (—) and T_s (-···) at frequencies of (a) 0.1; (b) 0.2; (c) 0.4 and (d) 0.8 rad/s. For these simulations, h is taken as 400 W/m^2 K.

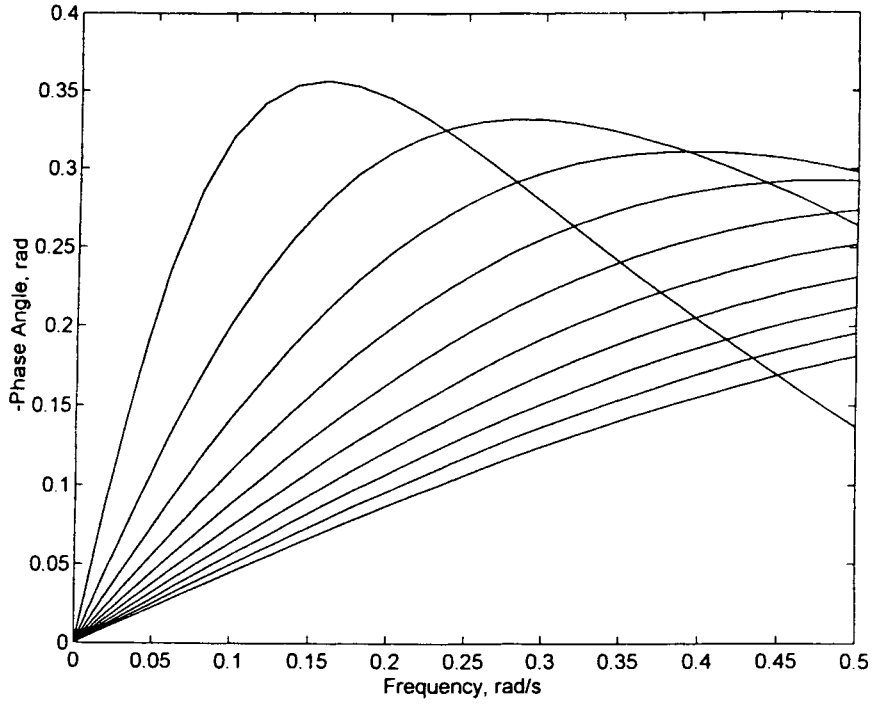

Fig. 4. The effect of k_σ on the phase angle. Values of k_σ vary between 0.2 W/m K (top) and 2.0 W/m K (bottom) with an interval of 0.2 W/m K.

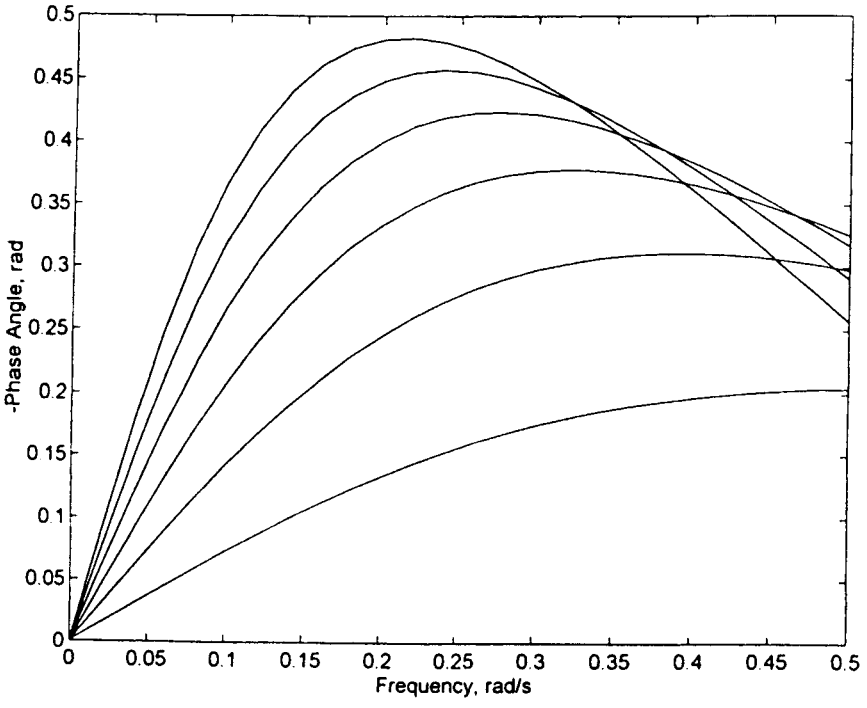

Fig. 5. The effect of sample thickness on the phase angle. Thickness ranges between 0.25 mm (bottom) and 1.50 mm (top) with an interval of 0.25 mm. For these simulations, h is taken as 2000 W/m^2 K.

value of $-\phi_{\sigma s}$, which appears at increasingly higher frequency. The performance of the TMDSC instrument will therefore be optimised, as far as the phase angle is concerned, by using a sensor with as high a thermal conductivity as possible.

Considering now the influence of the sample itself, the effect of sample thickness on the phase angle at different modulation frequencies can be seen in Fig. 5. Here it is assumed that the interface between sample and sensor is identical for all these samples, a situation that is, however, not always easy to achieve in practice, and which is discussed later. At low frequency, $-\phi_{\sigma s}$, increases with increasing sample thickness However, the non-linearity in the dependence of $-\phi_{\sigma s}$ on frequency, noted earlier, means that the increase is not linearly proportional to the thickness; looking at the phase angles corresponding to $\omega = 0.1$ rad/s for example, one can see that a linear relationship between $-\phi_{\sigma s}$ and sample thickness exists only for thickness less than or equal to 0.5 mm. This non-linearity can be explained by the presence of the quantity R (Eq. (A.15)) in Eq. (A.28) for the phase angle: increasing sample thickness increases R as well as increasing P, which simultaneously reduces the term $(1-\omega^2 QR)$ in the numerator and increases the denominator in Eq. (A.28), thus reducing $-\phi_{\sigma s}$. At higher frequencies, a maximum in $-\phi_{\sigma s}$ is observed to occur at a frequency that reduces as the sample thickness increases, whilst the magnitude of the negative phase angle increases. In fact, these results are somewhat unrealistic, particularly for the thickest samples, since the samples are all assumed to be at a uniform temperature, whereas in practice there will be a temperature gradient within the sample, and this will be most marked for the thickest samples. A further refinement of the present model, taking into account temperature gradients in the sample, is currently in preparation.

Despite this lack of refinement in the present model, it is possible to make some qualitative, or even semi-quantitative, observations from the curves in Fig. 5. It is clear that increasing the frequency for any sample thickness causes $-\phi_{\sigma s}$ to pass through a maximum and then to decrease towards zero and even for $\phi_{\sigma s}$ to reach

positive values, though this is not shown in Fig. 5. The cross-over for $\phi_{\sigma s}$ from negative to positive values occurs, from Eq. (A.28), when $\omega^2 = 1/(QR)$, as discussed above in the context of the heat transfer coefficient (refer to Fig. 2). Since R (Eq. (A.15)) is linearly proportional to sample thickness, this means that the cross-over frequency will decrease as sample thickness increases. Thus, whereas the curves for the dependence of $-\phi_{\sigma s}$ on h, shown in Fig. 2, fan out as h increases, those for the dependence of $-\phi_{\sigma s}$ on sample thickness, shown in Fig. 5, must intersect as sample thickness increases. The predictions of the theoretical model for heat transfer presented above will now be compared with some experimental data obtained on glassy polycarbonate.

4.2. Experimental results

Although most of the results presented here have been obtained using a single amplitude of temperature modulations of 0.5 K, a series of quasi-isothermal experiments was performed at a fixed frequency of 0.05 rad/s, corresponding to a period of 120 s, with a single sample of mass 12.0 mg, corresponding to a thickness of 0.50 mm, and with a range of temperature amplitudes from 0.03 to 3.0 K. The results are shown in Fig. 6, from which it is clear that the phase angle is independent of amplitude of the temperature modulations, at least within the usual range of experimental values. The scatter observed in the values $-\phi_{\sigma s}$ for the smallest amplitudes of 0.03 and 0.05 K arises because, in quasi-isothermal experiments with such small temperature amplitudes, the magnitude of the measured heat flow is below the recommended lower limit at which the accuracy of the instrument becomes compromised. The observed independence of phase angle with respect to temperature amplitude is inherent in the model predictions, since the amplitude does not appear in any of the theoretical expressions for the phase angle, for example Eq. (A.28). Indeed, this same result emerged also from the earlier simple model (Eq. (7)).

Considering now the frequency dependence of the phase angle, Fig. 7 shows the variation $-\phi_{\sigma s}$ as a function of frequency up to just more than 0.5 rad/s (period = 12 s), for a range of sample thicknesses from 0.25 to 1.50 mm. It is immediately apparent that the relationship between $-\phi_{\sigma s}$ and ω is non-linear, in other words that the expression derived from the simple model (Eq. (7)) is inadequate, particularly if frequencies greater than, say, 0.1 rad/s are used. On the other hand, the non-linear dependence is very similar to that predicted by the present model (refer to Fig. 5): the negative phase angle increases with increasing sample thickness (i.e. with increasing sample mass); a similar range of phase angles is observed

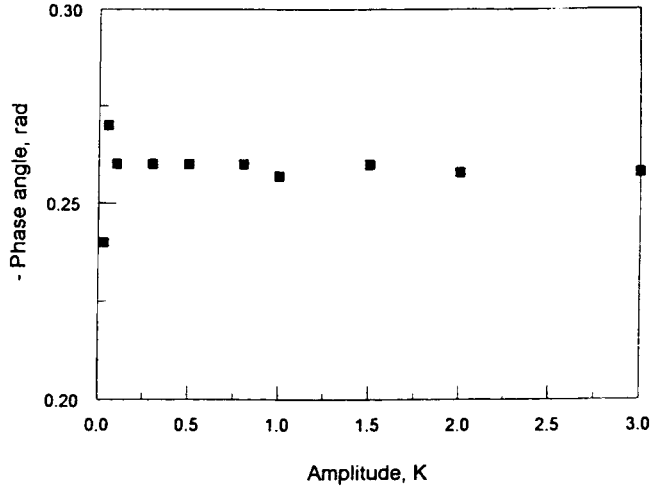

Fig. 6. The dependence of phase angle on amplitude of temperature modulation. The other experimental conditions were: $\omega = 0.05$ rad/s, sample mass = 12.0 mg. Note the expanded scale for the phase angle.

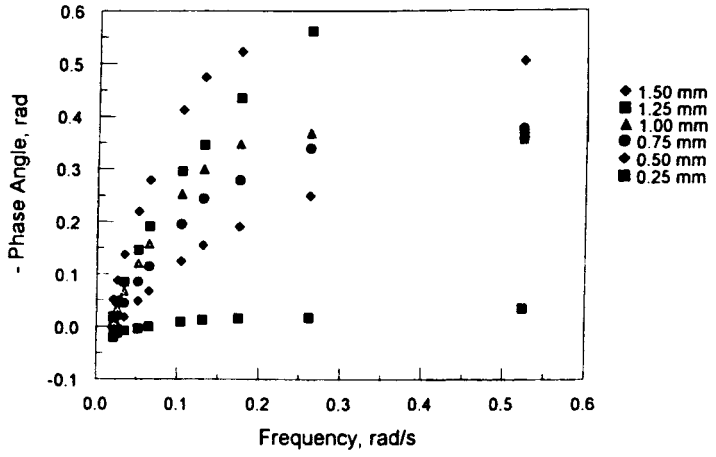

Fig. 7. Dependence of phase angle of polycarbonate on frequency in quasi-isothermal ADSC at 100°C, for various sample masses.

for the range of sample thickness used here; for each sample thickness, the negative phase angle levels off substantially at frequencies around 0.2 rad/s; and, finally, there is even some evidence for a possible reduction in the negative phase angle for the thickest samples at the highest frequencies.

The dependence of phase angle on sample thickness can be seen in Fig. 8, where the data have been cross-plotted from Fig. 7 at selected values of the frequency.

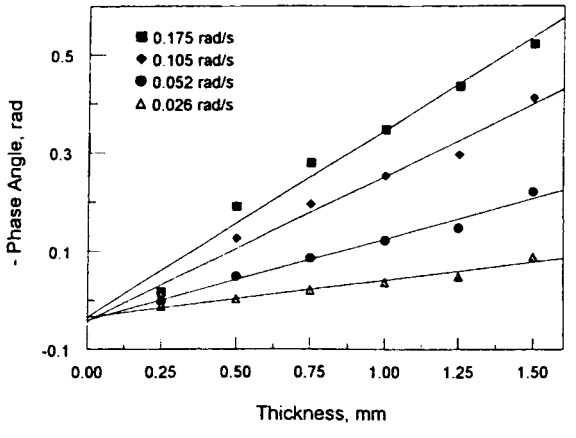

Fig. 8. Dependence of phase angle on the thickness (and hence mass) of polycarbonate samples using quasi-isothermal ADSC at 100°C, for selected modulation frequencies, cross-plotted from the data of Fig. 7. The straight lines represent the least squares fit to the sets of data corresponding to each frequency.

It can be seen that there is a reasonable linear relationship at each frequency, which implies that the "correction factors" in the numerator and denominator of Eq. (A.28) have a much smaller influence in respect of the sample mass than they do in respect of the frequency. This would, in fact, be anticipated from Eq. (A.28), since the frequency ω enters these "correction factors" as either ω^2 or ω^4 whereas the sample mass enters (either through P or R, Eqs. (A.13) and (A.15), respectively) only as a linear or as a square term, respectively, or with a reduced influence by virtue of the presence of other terms, as in the ω^2 term of the denominator of Eq. (A.28). Additionally, there is likely to be more scatter in the data presented in Fig. 8, because for each sample thickness a different sample needed to be used. This introduced the possibility of different heat transfer coefficients, which creates another complication to be discussed further below. It is interesting to note in Fig. 7 that the curves do not pass through the origin; there is a clear indication that they converge at a small positive phase angle as the frequency approaches zero. This is contrary to the prediction of the model in Eq. (A.28), where the phase angle is zero for a frequency of zero. It is believed, however, to be a consequence of the calibration procedure followed here, and is currently being investigated.

In order to determine the effect on the phase angle of the interface between the sensor and the sample, for comparison with the theoretical predictions shown

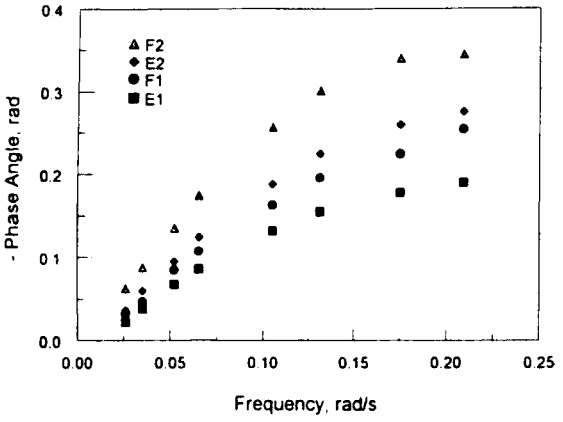

Fig. 9. Dependence of phase angle on frequency for different polycarbonate samples using "head and tail" measurements. E1 – head, 12.62 mg; E2 – tail, 12.62 mg; F1 – head, 12.95 mg; F2 – tail, 12.95 mg.

in Fig. 2, we would ideally like to prepare samples with different surface finishes such that a range of heat transfer coefficients can be examined experimentally. This is not easy, however. Instead, so-called "head and tail" experiments have been performed, as follows. During the specimen machining process, in which samples were parted off from the 5 mm diameter rod, it is inevitable that the quality of the machined surface on each side of the disc-shaped sample is different. This gives rise to samples with "head and tail" surfaces, which affords the opportunity of measuring the ADSC response for identical samples with different (but unquantified) heat transfer coefficients.

The results are shown in Fig. 9, where the negative phase angle is plotted as a function of frequency for two samples, E and F, with sample masses 12.62 and 12.95 mg, respectively, in each of the two orientations. It is clear that the quality of surface finish has a marked effect on the phase angle over the whole range of frequencies, increasing the magnitude of the phase angle on going from "heads" to "tails" by approximately the same amount for each sample at any given frequency. Hence, changing sample mass by changing the sample is likely to introduce extraneous effects from different surface finishes, and will give a certain amount of scatter in the experimental data for the dependence of phase angle on sample thickness (Fig. 8), for example. More generally, whenever different samples are compared in ADSC in respect of their phase angles, this possible source of error must be borne in mind.

One possible way to overcome this effect is to introduce between the sensor and the sample (in practice between the sample and the aluminium pan) a heat transfer fluid such that the heat transfer coefficient is always the same (albeit unknown) whatever the quality of the surface finish of the sample. In order to examine this possibility, we introduced here a drop of silicone oil between sample and aluminium pan. For these measurements, though, the ADSC calibration procedure had to be modified slightly, otherwise the blank run would have made an incorrect on-line calibration of the heat capacity on the basis of a difference between sample and reference side which included both an aluminium lid and a drop of silicone oil. Thus, three separate ADSC runs were performed as follows: (1) empty run - without crucibles (pans) in either sample or reference positions; (2) blank run - a crucible plus lid, containing a drop of silicone oil, on the sample side, and a crucible without lid, but with (as closely as was possible) the same amount of silicone oil, on the reference side; (3) sample run - the same crucible plus lid, with the oil (as for 2) and now with the polycarbonate sample, on the sample side, and the same crucible without lid but with silicone oil (as for 2) on the reference side.

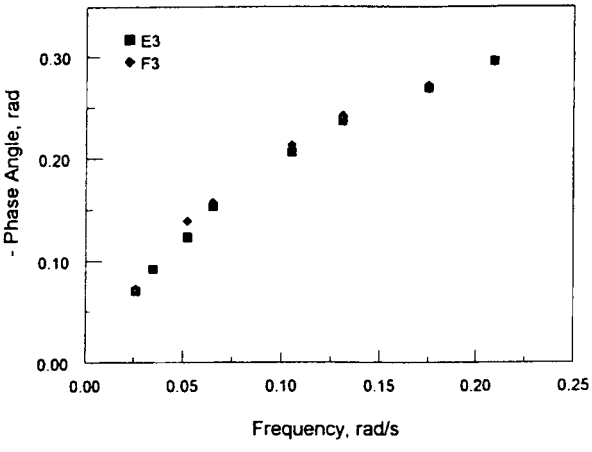

Fig. 10. Dependence of phase angle on frequency for polycarbonate plus silicone oil by quasi-isothermal measurements. E3 – polycarbonate, 12.62 mg, plus silicone oil, 2.82 mg; F3 – polycarbonate, 12.95 mg, plus silicone oil, 0.30 mg.

The results of this experiment, using the same samples E and F as earlier, are shown in Fig. 10 for the negative phase angle as a function of frequency. In this case, the samples E and F were in the ''heads'' orientation; and therefore these results should be compared with those for El and F1 in Fig. 9. Two effects are apparent. First, the magnitude of the phase angle increases when the silicone oil is introduced, which implies that the heat transfer coefficient is increased by the introduction of this liquid at the interface between sample and aluminium pan. The second, and more important, effect is that the data for the two samples, E and F, now superpose in Fig. 10 where they did not in Fig. 9. The implication is that a reproducible heat transfer between sample and aluminium pan can be achieved, even with samples which have different surface finishes. Furthermore, this effect is achieved with quite different masses of silicone oil (2.82 mg for sample E and 0.30 mg for sample F), provided that the appropriate procedure described above is followed during the calibration. Note that the small difference in sample masses between E and F (<3%) would give rise to a phase angle difference of less than 0.01 rad, and hence within the experimental error of the data in Fig. 10.

5. Conclusions

A new theoretical approach has been developed in which the phase angle between reference and sample side sensors in ADSC is examined under various conditions. The corresponding quasi-isothermal experimental results have revealed several features of the ADSC experiments. (1) The theoretical predictions and the experimental results are in good agreement, and show that the phase angle is not only determined by the sample properties, but is also strongly affected by the heat transfer between sample and pan. (2) The introduction of a small amount of heat transfer fluid between sample and pan improves the heat transfer and largely eliminates the variations in phase angle due to the different qualities of the sample surfaces, provided that an appropriate calibration procedure is followed. (3) The phase angle is independent of modulation amplitude, as predicted theoretically.

Acknowledgements

We gratefully appreciate Aberdeen University Research Committee and Mettler-Toledo for financial support of this work.

Appendix A

Derivation of expressions for a, b, d and e (subscripted 1 and 2) for Model B (refer to Eqs. (9) and (10))

The equations for the sample side sensor temperature, $T_{\sigma s}$, and for the sample temperature, T_s, are given in Eqs. (9) and (10). From Eqs. (15), (16) and (17) we may then find:

$$\frac{k_{\sigma s}A}{L_{\sigma s}}(T_d - T_{\sigma s}) = m_s C_{p,s}\dot{T}_s + m_{\sigma s}C_{p,\sigma s}\dot{T}_{\sigma s} \quad (A.1)$$

and Eq. (16) is

$$h \cdot A(T_{\sigma s} - T_s) = m_s C_{p,s}\dot{T}_s,$$

where T_d is given by Eq. (14). Substituting Eqs. (9) and (10) into Eqs. (A.1) and (16), and equating coefficients, gives the following equations. Note that we are ignoring here the terms with coefficients c_1 and c_2 in Eqs. (9) and (10), respectively. The reason for this is that these terms represent transient effects, whereas we are interested here only in steady state conditions.

1. *Constant coefficients*:

$$\frac{k_{\sigma s}A}{L_{\sigma s}}\left(T_0 + \frac{m_{\sigma r}C_{p,\sigma r}L_{\sigma r}}{k_{\sigma r}A}\beta - a_1\right) = m_s C_{p,s}b_2 + m_{\sigma s}C_{p,\sigma s}b_1, \quad (A.2)$$

$$hA(a_1 - a_2) = m_s C_{p,s}b_2. \quad (A.3)$$

2. *Coefficients of t*:

$$\frac{k_{\sigma s}A}{L_{\sigma s}}(\beta - b_1) = 0, \quad (A.4)$$

$$hA(b_1 - b_2) = 0. \quad (A.5)$$

3. *Coefficients of sin ωt*:

$$\frac{k_{\sigma s}A}{L_{\sigma s}}(A_T - d_1) = m_s C_{p,s}(-\omega e_2) + m_{\sigma s}C_{p,\sigma s}(-\omega e_1), \quad (A.6)$$

$$hA(d_1 - d_2) = m_s C_{p,s}(-\omega e_2). \quad (A.7)$$

4. *Coefficients of cos ωt*:

$$\frac{k_{\sigma s}A}{L_{\sigma s}}\left(\frac{m_{\sigma r}C_{p,\sigma r}L_{\sigma r}}{k_{\sigma r}A}\omega A_T - e_1\right) = m_s C_{p,s}(\omega d_2) + m_{\sigma s}C_{p,\sigma s}(\omega d_1), \quad (A.8)$$

$$hA(e_1 - e_2) = m_s C_{p,s}(\omega d_2). \quad (A.9)$$

From Eqs. (A.4) and (A.5), one finds:

$$b_1 = b_2 = \beta. \quad (A.10)$$

It is now assumed that the sensors on the reference and sample sides are identical, so that $m_{\sigma r} = m_{\sigma s} = m_\sigma$, $C_{p,\sigma r} = C_{p,\sigma s} = C_{p,\sigma}$, $L_{\sigma r} = L_{\sigma s} = L_\sigma$ and $k_{\sigma r} = k_{\sigma s} = k_\sigma$. From Eqs. (A.2) and (A.3) one can then find

$$a_1 = T_0 = \frac{m_s C_{p,s} L_\sigma}{k_\sigma A}\beta \quad (A.11)$$

and

$$a_2 = T_0 - \frac{m_s C_{p,s} L_\sigma}{k_\sigma A}\beta - \frac{m_s C_{p,s}}{hA}\beta. \quad (A.12)$$

Writing the following combinations, all of which have dimensions of time

$$P = \frac{m_s \cdot C_{p,s} \cdot L_\sigma}{k_\sigma \cdot A}, \quad (A.13)$$

$$Q = \frac{m_\sigma \cdot C_{p,\sigma} \cdot L_\sigma}{k_\sigma \cdot A}, \quad (A.14)$$

$$R = \frac{m_s \cdot C_{p,s}}{h \cdot A} \quad (A.15)$$

then Eqs. (A.11) and (A.12) reduce to

$$a_1 = T_0 - P\beta, \quad (A.16)$$

$$a_2 = T_0 - (P + R)\beta \quad (A.17)$$

and Eqs. (A.6) and (A.9) may be simplified to

$$d_1 - \omega Q e_1 - \omega P e_2 = A_T, \quad (A.18)$$

$$d_1 - d_2 + \omega \mathrm{Re}_2 = 0, \quad (A.19)$$

$$\omega Q d_1 + \omega P d_2 + e_1 = \omega Q A_T, \quad (A.20)$$

$$\omega \mathrm{R} d_2 - e_1 + e_2 = 0, \quad (A.21)$$

which may be expressed in matrix form as

$$\begin{bmatrix} 1 & 0 & -\omega Q & -\omega P \\ 1 & -1 & 0 & \omega R \\ \omega Q & \omega P & 1 & 0 \\ 0 & \omega R & -1 & 1 \end{bmatrix} \begin{bmatrix} d_1 \\ d_2 \\ e_1 \\ e_2 \end{bmatrix} = \begin{bmatrix} 1 \\ 0 \\ \omega Q \\ 0 \end{bmatrix} A_T. \quad (A.22)$$

The solution of the above equations can be found as

$$d_1 = \frac{1+\omega^2(PQ+PR+Q^2+R^2)+\omega^4Q^2R^2}{1+\omega^2(P^2+2PQ+Q^2+2PR+R^2)+\omega^4Q^2R^2}A_T, \quad (A.23)$$

$$d_2 = \frac{1+\omega^2Q(P+Q)}{1+\omega^2(P^2+2PQ+Q^2+2PR+R^2)+\omega^4Q^2R^2}A_T, \quad (A.24)$$

$$e_1 = -\frac{\omega P(1-\omega^2QR)}{1+\omega^2(P^2+2PQ+Q^2+2PR+R^2)+\omega^4Q^2R^2}A_T, \quad (A.25)$$

$$e_2 = -\frac{\omega(P+R+\omega^2Q^2R)}{1+\omega^2(P^2+2PQ+Q^2+2PR+R^2)+\omega^4Q^2R^2}A_T. \quad (A.26)$$

Note that the numerators of d_1 (Eq. (A.23)) and d_2 (Eq. (A.24)) are both smaller than their respective denominators, and hence both d_1 and d_2 are less than A_T, the latter more so than the former.The sample side sensor temperature may therefore be written in the steady state as

$$T_{\sigma s} = T_0 + \beta(t - P) + A_{\sigma s}\sin(\omega t + \phi_{\sigma s}), \quad (A.27)$$

where $A_{\sigma s} = \sqrt{d_1^2 + e_1^2}$ and $\phi_{\sigma s}$ is the phase angle of the sensor temperature on the sample side relative to that on the reference side (the reference leading the sample) and is given by

$$\phi_{\sigma s} = \arctan\left(\frac{e_1}{d_1}\right) = \arctan\left[\frac{-\omega P(1-\omega^2QR)}{1+\omega^2(PQ+PR+Q^2+R^2)+\omega^4Q^2R^2}\right]. \quad (A.28)$$

In the limit of low frequencies, $A_{\sigma s} \approx A_T$ and $\phi_{\sigma s} \approx \arctan(-\omega P)$.

The sample temperature itself may likewise be written in the steady state as

$$T_s = T_0 + \beta(t - P - R) + A_s \sin(\omega t + \phi_s) \tag{A.29}$$

where $A_s = \sqrt{d_2^2 + e_2^2}$ and ϕ_s is the phase angle of the sample temperature relative to the reference sensor temperature (the reference leading the sample) and is given by

$$\phi_s = \arctan\left(\frac{e_2}{d_2}\right) = \arctan\left[-\frac{\omega(P + R + \omega^2 Q^2 R)]}{1 + \omega^2 Q(P + Q)}\right]. \tag{A.30}$$

In the limit of low frequencies, $A_s \approx A_T$ and $\phi_s \approx \arctan[-\omega(P+R)]$.

References

[1] M. Reading, Trends Polym. Sci. 1 (1993) 248.
[2] P.S. Gill, S.R. Sauerbrunn, M. Reading, J. Thermal Anal. 40 (1993) 931.
[3] M. Reading, D. Elliott, V.L. HiII, J. Thermal Anal. 40 (1993) 949.
[4] J.E.K. Schawe, Thermochim. Acta 261 (1995) 183.
[5] A. Boller, C. Schick, B. Wunderlich, Thermochim. Acta 266 (1995) 97.
[6] A. Boller, I. Okazaki, B. Wunderlich, Thermochim. Acta 284 (1996) 1.
[7] I. Okazaki, B. Wunderlich, J. Polym. Sci. B 34 (1996) 2941.
[8] A. Hensel, J. Dobbertin, J.E.K. Schawe, A. Boller, C. Schick, J. Thermal Anal. 46 (1996) 935.
[9] J.M. Hutchinson, S. Montserrat, J. Thermal Anal. 47 (1996) 103.
[10] J.M. Hutchinson, S. Montserrat, Thermochim. Acta 286 (1996) 263.
[11] J.M. Hutchinson, S. Montserrat, Thermochim. Acta 304 305 (1997) 257.
[12] J.E.K. Schawe, G.W.H. Höhne, J. Thermal Anal. 46 (1996) 893.
[13] M. Song, A. Hammiche, H.M. Pollock, D.J. Hourston, M. Reading, Polymer 36 (1995) 3313.
[14] M. Song, A. Hammiche, H.M. Pollock, D.J. Hourston, M. Reading, Polymer 37 (1996) 5661.
[15] G. Van Assche, A. Van Hemelrijck, H. Rahier, B. Van Mele, Thermochim. Acta 286 (1996) 209.
[16] G. Van Assche, A. Van Hemelrijck, H. Rahier, B. Van Mele, Thermochim. Acta 304 305 (1997) 317.
[17] Z. Jiang, J.M. Hutchinson, C.T. Imrie, Polym. Inter. 47 (1998) 72.
[18] B. Wunderlich, Y. Jin, A. Boller, Thermochim. Acta 238 (1994) 277.
[19] S. Weyer, A. Hensel, C. Schick, Thermochim. Acta 304 305 (1997) 267.
[20] J.E.K. Schawe, W. Winter, Thermochim. Acta 298 (1997) 9.
[21] Z. Jiang, C.T. Imrie, J.M. Hutchinson, Thermochim. Acta 315 (1998) 1.